SCIENTIFIC REPORTS

OPEN

Employing graphene acoustoelectric switch by dual surface acoustic wave transducers

Received: 6 March 2019
Accepted: 20 May 2019
Published online: 03 June 2019

Ching-Ping Lee[1], Yu-Peng Hong[1], Man-Ting Shen[1], Chiu-Chun Tang[1], D. C. Ling[2], Yung-Fu Chen[3], Cen-Shawn Wu[4] & Jeng-Chung Chen[1]

We implement a logic switch by using a graphene acoustoelectric transducer at room temperature. We operate two pairs of inter-digital transducers (IDTs) to launch surface acoustic waves (SAWs) on a $LiNbO_3$ substrate and utilize graphene as a channel material to sustain acoustoelectric current I_{ae} induced by SAWs. By cooperatively tuning the input power on the IDTs, we can manipulate the propagation direction of I_{ae} such that the measured I_{ae} can be deliberately controlled to be positive, negative, or even zero. We define the zero-crossing I_{ae} as I_{ae}^{off}, and then demonstrate that I_{ae} can be switched with a ratio $I_{ae}^{on}/I_{ae}^{off} \sim 10^4$ at a rate up to few tens kHz. Our device with an accessible operation scheme provides a means to convert incoming acoustic waves modulated by digitized data sequence onto electric signals with frequency band suitable for digital audio modulation. Consequently, it could potentially open a route for developing graphene-based logic devices in large-scale integration electronics.

Graphene –a two-dimensional (2D) sheet of carbon atoms arranged in a honeycomb lattice– exhibits various unique properties beneficial for post-silicon electronics[1,2]. Recent developments in graphene field-effect transistors (GFETs) suggest that graphene holds great promise in radio frequency (RF) applications[3–5]. For digital electronics, adopting new materials as a successor to Si must perform excellent switching capabilities with a low off-state dissipation power and a high on/off current ratio[6,7]. Nevertheless, graphene shows a serious hurdle for its applications in logic circuits[2], because the pristine graphene does not possess an energy bandgap[1]. As a result, GFET cannot be turned off efficiently, leading to a low on/off current ratio typically less than 10^2. Subsequently, the research efforts are geared toward two different directions: engineering graphene material to open a bandgap[8,9], or exploiting layered 2D semiconductors with a naturally occurring bandgap, e.g. transition metal dichalcogenides (TMDs) and black phosphorus (BP)[7].

In this work, we report a different approach to implementing graphene for logic devices by utilizing acoustoelectric effects. Here graphene is used as a channel material to convert surface acoustic wave (SAW) into acoustoelectric current I_{ae}. We will show that I_{ae} induced by dual SAWs can be modulated by discretizing RF signals. In this regard, a graphene acoustoelectric transducer(GAET) can function as a logic switch. The switching performance is demonstrated by the successful generation and detection of the digital text carried by I_{ae} with a switching rate up to few tens kHz.

A surface acoustic wave is an acoustic wave traveling along the surface of the piezoelectric materials, with its displacement amplitude exponentially decaying into the material so that it is roughly confined within one wavelength beneath the surface[10]. SAW can be induced by distributed comb-like metallic structures, such as inter-digital transducers (IDTs), deposited on the surface of the piezoelectric substrate. Triggered by the piezoelectric effect, the RF input signal at the transmitting IDT stimulates the SAW. For a typical SAW device, a second IDT is employed, served as a signal processing unit and a transducer, to convert the acoustic waves back into a RF signal. Nowadays, the SAW devices have been widely used in various RF signal processing techniques for telecommunications and sensors[11,12].

The propagation of SAW is sensitively influenced by the local changes of the host medium, which causes the variations of the SAW velocity v_s and the SAW attenuation factor Γ. For example, SAWs can interact with

[1]Department of Physics, National Tsing Hua University, Hsinchu, 30013, Taiwan. [2]Department of Physics, Tamkang University, Tamsui Dist., New Taipei City, 25137, Taipei, Taiwan. [3]Department of Physics, National Central University, Jhongli, 32001, Taiwan. [4]Department of Physics, National Changhua University of Education, Changhua, 50007, Taiwan. Correspondence and requests for materials should be addressed to C.-P.L. (email: chingping1984@gmail.com)

two-dimensional electron gas (2DEG) placed nearby and the corresponding changes in both v_s and Γ have been used to probe the distinct electronic states of 2DEG[13–16]. In addition, the interaction between the SAW and the charge carriers of 2DEG can also induce a macroscopic direct current, acoustic current I_{ae}, which is known as the acoustoelectric effect.

The acoustoelectric properties of graphene have been extensively studied[17–25]. Owning to the linear energy dispersion and gapless nature of graphene, electrons in graphene can absorb sound waves over a wide frequency range[26] and in theory Γ is strikingly diminished as the Fermi level E_F is tuned across the charge neutral point (CNP)[17,20]. However, graphene does not possess piezoelectricity because of its central symmetric lattice structure, unlike to GaAs-2DEG. The major obstacles in studying and utilizing the acoustoelectric effects of graphene lie on how to generate SAW and maintain its propagation under the control of E_F. Early experiments reveal that SAW of graphene can be excited by placing graphene either on or in close contact to a substrate with high piezoelectricity, e.g. $LiNbO_3$ substrate[18]. By incorporating ion liquid gate and IDTs, E_F of graphene can be tuned across CNP, and I_{ae} exhibits an ambipolar effect- the sign of I_{ae} is reversed associated with the change of charge carriers from n- to p-type[22,23]. Furthermore, Γ of grapehene is extremely weak, approximately ~0.4 to 6.8 m^{-1} depending on the carrier density n_s, which is three orders of magnitude smaller than that of GaAs 2DEG systems[23]. These fascinating properties make graphene an ideal material for various acoustoelectric devices, ranging from acoustic tweezers, branch switch, flip-chip devices etc.[22,27–29].

A theoretical model to describe acoustodynamic effects in semiconductors was developed by G. Weinreich[30]. The acoustic current in a closed-circuit measurement (or voltage in an open-circuit measurement) is induced by a loss of wave energy associated with a proportional loss of SAW momentum, which is analogous to a force applying on the absorber (the charge carriers of graphene in this study). For a 2D system, we can assume that the acoustic current density j^{ae} is proportional to Γ with the coefficient Λ and flows along the direction of SAW propagation[15,16,31]:

$$j_i^{ae} = \Lambda I_i \Gamma / v_s, \tag{1}$$

here $i(=x$ or $y)$ is the spatial index, $I_{x(y)}(=I^0_{x(y)}\exp(-\Gamma x(y))$ is the intensity of the SAW propagating along the $x(y)$-direction. It has been known that Λ can be described by[16]

$$\Lambda = \sigma / n_s e, \tag{2}$$

where σ is the DC conductivity of graphene. We assume that both Γ and Λ are spatially uniform because graphene is an isotropic material. Note that one may need to treat Γ and Λ in a tensor form when the SAW propagates on an anisotropic substrate or the carriers are in the presence of an external magnetic field[15,16,31].

Because of the ambipolar effect of graphene, j_i^{ae} through graphene in the electron- and hole-rich regimes flows in opposite direction and vanishes at charge neutral region due to cancellation[22,23]. Consequently, one can define a true zero-current state or an "off"-state at CNP although the channel is not completely closed. On the other hand, a fair on/off ratio ~20 has been reported by defining an on/off state away from CNP in our earlier study[23]. In principle, if the off-state is set exactly at CNP, one can get a much higher ratio ($>10^7$). There are competitive advantages to utilize GAET for logic devices. For commercial SAW filters used in the RF front-end, the device requires sufficient high-power durability. In general the SAW device can withstand power levels $\geq$30 dBm, which is high enough to generate I_{ae} with a decent S/N ratio. Moreover, no quiescence power source is needed because GAET is activated by the energy of the RF input signals received by the IDT transceiver. Nevertheless, if one operated GAET like GFET that the RF signal is sent through the gate electrode[3,4], the modulation speed of GAET would be too slow for practical applications[23]. It is mainly because the ionic liquid is adopted for the gate electrode in the present GAET design[22,23]. Note that the gate electrode made of conducting materials will severely damp the propagation of SAWs. This is the key bottleneck for GAET to be used for the logic devices.

Design Concept and Device Details

Our design concept is illustrated in Fig. 1(b). Two IDTs, denoted as IDT1 and IDT2, are employed on a $LiNbO_3$ piezoelectric substrate in a nearly orthogonal arrangement. Each IDT comprises two sets of interleaved fingers and the acoustic current density induced by IDT1 and IDT2 is indicated as j^{IDT1} and j^{IDT2}, respectively. Two current sensing leads are placed along the positive x-direction (cf. Fig. 1), and the measured acoustic current I_{ae} is determined by the vector sum of j_{+x}^{IDT1} and j_{-x}^{IDT2}. The negative x-component of j^{IDT2} can be induced by deliberately adjusting orientation of IDTs or simply by the imperfection of the device. Therefore, we can manipulate the flow of I_{ae} by controlling the RF power separately applied on IDT1 and IDT2. As a result, the magnitude of I_{ae} measured could be positive, negative, or even zero. Our approach can be viewed as an application of acoustic-based active mixing technique, which has been widely used in studies of microfluidic channels with I_{ae} acting as the acoustic streaming of the sample liquid[32]. To make analogue to operation method of conventional field-effect transistor(FET), IDT1 functions as the source contact to inject the channel current and IDT2 serves as a gate electrode to turn "on/off" the device. We will demonstrate below that by digitizing RF signal applied on IDT2 or IDT1, the GAET can perform as a logic switch.

Figure 2(a) shows a schematic diagram of the investigated GAET. The device consists of two pairs of IDTs, denoted as IDT1 to IDT4, on $LiNbO_3$ substrate, graphene, four electrodes on graphene labeled as leads 1 to 4, and a micro-bead of an ion-gel coated on graphene[33], a gate electrode of the polymer electrolyte for applying gate voltage V_g. The two sets of opposite ITDs, IDT1-IDT3 and IDT2-IDT4, are separated with a distance $L_T = 1.4$ mm and backed by metallic strips to damp reflected waves. In this study, we only operate IDT1 and IDT2, and conduct their counterpart IDT3 and IDT4 as a passive receiver for checking the SAW properties. Each IDT comprises two sets of interleaved fingers with $N_{IDT} = 25$ finger pairs made by 5 μm wide electrodes with 8/70 nm of Cr/Au. The

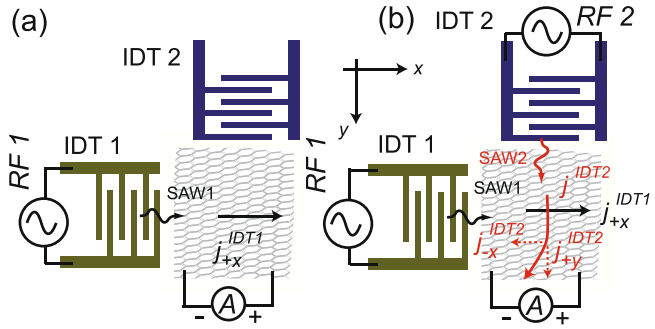

Figure 1. Schematics of the design concept for graphene acoustoelectric transducer (GAET). (**a**) The acoustoelectric current j^{IDT1}_{+x} in graphene is generated by IDT1 and measured along the positive x-direction. (**b**) Both IDT1 and IDT2 are activated by two different RF signals. The measured acoustoelectric current is the sum of j^{IDT1}_{+x} and j^{IDT2}_{-x}. Here we consider that graphene is in the hole-rich regime and its Fermi level is tuned away from the charge neutral point (CNP).

acoustic aperture $W_T \sim 600\,\mu$m, the overlap between electrodes, is aligned between two opposite IDTs along the [011] direction of the z-cut single-crystal $LiNbO_3$ substrate. The optical micrograph of device can be found in the Fig. 2(d,e). The SAW wavelength λ_{SAW} determined by the pitch of the IDT electrode is 20 μm and the SAW velocity v_s is approximately 3795 m/s[34]. The central resonance frequency $f = v_s/\lambda_{SAW}$ is estimated to be 190 MHz. Figure 2(b) shows the transmittance S_{21} as a function of frequency measured by a network analyzer (RS ZVA24). It exhibits a peak at approximately central frequency $f_c = 191$ and 187 MHz for IDT1 → IDT3 and IDT2 → IDT4 respectively, which fairly agrees with the designed value.

Graphene is prepared by the chemical vapor deposition. We refer the readers to our previous publications for the details of graphene growth, characterization, and transfer procedures[35–37]. Graphene is gently placed between two IDTs, and tailored to a rectangular shape of length $L_G = 600\,\mu$m and of width $W_G = 400\,\mu$m. Caution must be taken to ensure that graphene residues will not short the Au electrodes of IDTs. Four electrodes deposited along the side border of graphene are used for resistance and acoustoelectric current measurements. They are made of an Au/Cr bilayer with 8/70 nm in thickness and 20 μm in width, among which 450 μm in length for leads 1 and 4, and 250 μm in length for leads 2 and 3 (see Fig. 2(a)). Finally, a micro-bead of the solid polymer electrolyte, poly ethylene oxide (PEO) and $LiClO_4$[33], is dropped onto graphene surface with size slightly larger than graphene area. Note that the geometry of the electrodes is designed in a way that the damping effect on SAWs due to intruding into the metallic electrodes is minimized and I_{ae} flowing along either longitudinal or transverse direction can be collected as much as possible. Figure 2(c) shows the representative resistance $R(=V_{24}/I_{13})$ of graphene as a function of V_g, where V_{24} is the voltage measured across the lead 2 and 4, and I_{13} is the current passing through the lead 1 to 3. The R versus V_g trace of graphene reaches a maximum with resistance ~2.5 kΩ at CNP, where $V_g \equiv V_{CNP} = -0.549$ V. We have measured five devices with the same structures and got consistent results. Data presented below are mainly obtained from one of the devices.

Results and Discussion

The acoustoelectric characteristics of the studied devices at room temperature is shown in Fig. 3. Figure 3(a) displays the experimental setup of I_{ae} measurement. Here we use IDT1 and IDT2 to generate the SAWs and take leads 4 and 1 to sense I_{ae}, while keep the rest IDTs and electrodes inactive and open. We modulate RF signal at a frequency of 10 kHz and employ standard lock-in technique to measure I_{ae}. Note that the propagation direction of the I_{ae} measured by leads 4 and 1 aligns with that of the SAWs induced by IDT1. Figure 3(b) shows I_{ae} as a function of bias voltage V_g with various RF powers P_{IDT1} applied on IDT1 at the central frequency of 191 MHz, while keeping IDT2 inactive. With the present arrangement of the current leads displayed in Fig. 3(a), the measured I_{ae} is positive, negative, or zero as graphene is biased in the hole-rich regime, electron-rich regime, or at $V_g \sim V_{CNP}$. The gate bias dependence of I_{ae} manifests the unique Dirac dispersion relation of graphene[22,23]. We note that an on/off ratio of I_{ae} up to 10^7 can be achieved, for example, if one defines the on-state at $V_g - V_{CNP} = 0.5$ V and the off-state at $V_g = V_{CNP}$ for $P_{IDT1} = 10$ dBm. Extracted from Fig. 3(b), the measured acoustoelectric current as a function of the SAW intensity is plotted in Fig. 3(d). Within the applied RF power up to 10 dBm the acoustoelectric current is linearly proportional to the SAW intensity[18], as indicated in Eq. (1).

To present the performance of the device in the dual-SAW operation, we cooperatively activate IDT1 and IDT2 at frequency of 190 MHz. First, we launch the SAWs by IDT1 with a fixed $P_{IDT1} \sim -10$ dBm to induce a steady positive I_{ae} on graphene in the hole-rich regime, and then gradually increase the input RF power P_{IDT2} on IDT2 ranging from −10 dBm to 10 dBm. Figure 3(c) shows I_{ae} as a function of applied bias V_g with various P_{IDT2}. It is found that the value of I_{ae} decreases/increases with the increase of P_{IDT2} in the hole-/electron-rich regime. As $P_{IDT2} > 2$ dBm, I_{ae} almost diminishes. While P_{IDT2} increases further, I_{ae} remarkably changes sign, and its magnitude increases with P_{IDT2}. The evolution of I_{ae} with P_{IDT1} and P_{IDT2} is inconsistent with the mixing-flow of j^{ae} scenario described in Fig. 1(b). However, the experimental findings demonstrate that the dual-SAW operation can null acoustoelecctric current in a controllable manner, which provides an alternative route to turn "off" I_{ae}.

Next we will show that by dynamically controlling the on/off state of I_{ae}, GAET can be effectively operated as a logic switch. Figure 4(a) displays schematic diagram of the measurement circuit for real-time response

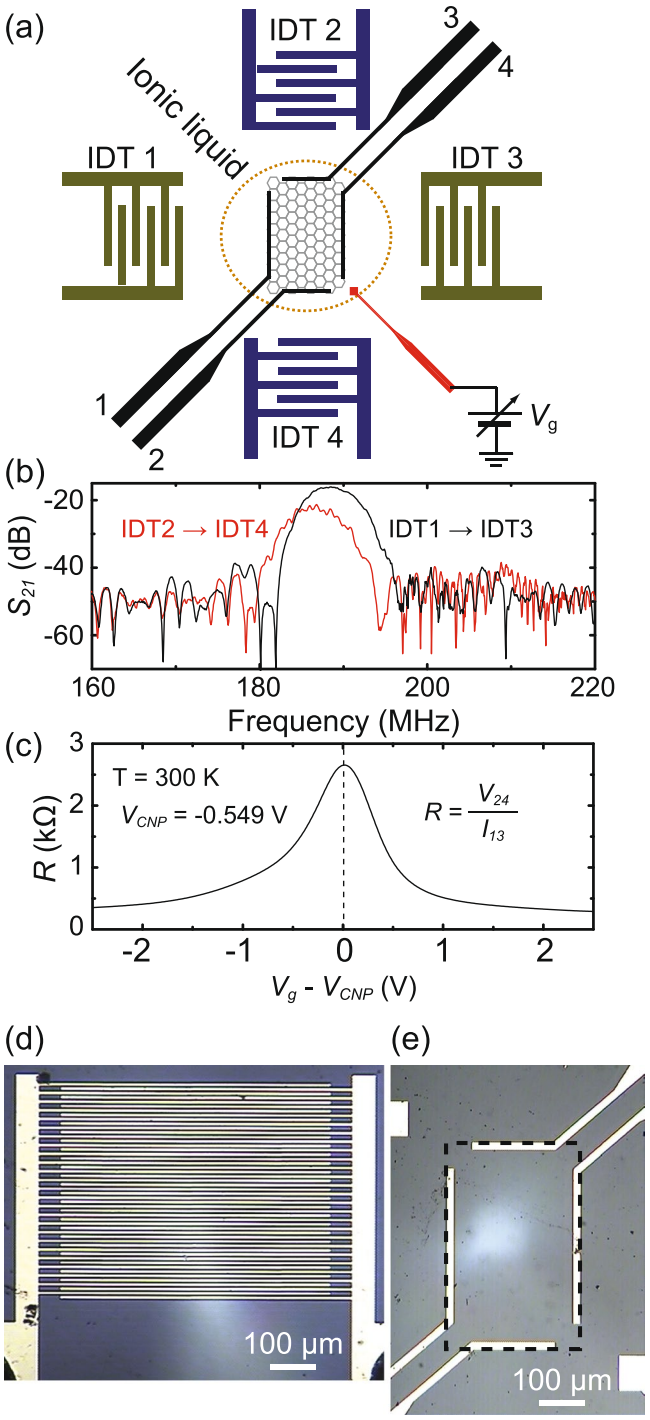

Figure 2. Device layout, characterizations and optical micrograph. (**a**) Schematic diagram of the studied GAET. (**b**) The transmission characteristics of SAWs taken with IDT1/IDT2 for launching SAW and IDT3/IDT4 for detection of SAW. It exhibits a peak at approximately 191 and 187 MHz, respectively. Here the input RF power is −10 dBm. (**c**) Graphene resistance R as a function of gate voltage V_g applied on the ionic liquid gate electrode. The resistance shows a maximum at the charge neutral point (CNP), where $V_g = -0.549$ V($\equiv V_{CNP}$). (**d**) The optical micrograph of IDT. Each IDT has 25 finger pairs made by 5 μm wide electrodes. The length of overlapped electrode is 600 μm. (**e**) The shape of graphene and the pattern of electrodes for graphene contacts. Graphene is tailored to a rectangular shape with 600 μm in length and 400 μm in width (frame with black dashed line). The longer electrodes are made with 450 μm in length, and the shorter electrodes are made 250 μm in length. All electrodes are made 20 μm in width.

measurements on I_{ae}. We first bias graphene in the hole-rich regime at $V_g - V_{CNP} = 0.5$ V and then simultaneously apply a constant $P_{IDT1} = -10$ dBm on IDT1 and a modulated P_{IDT2} on IDT2 to generate a time-varying I_{ae}. The open-circuit voltage V_{SAW} associated with the induced I_{ae} is amplified by a wide-band low noise amplifier and then

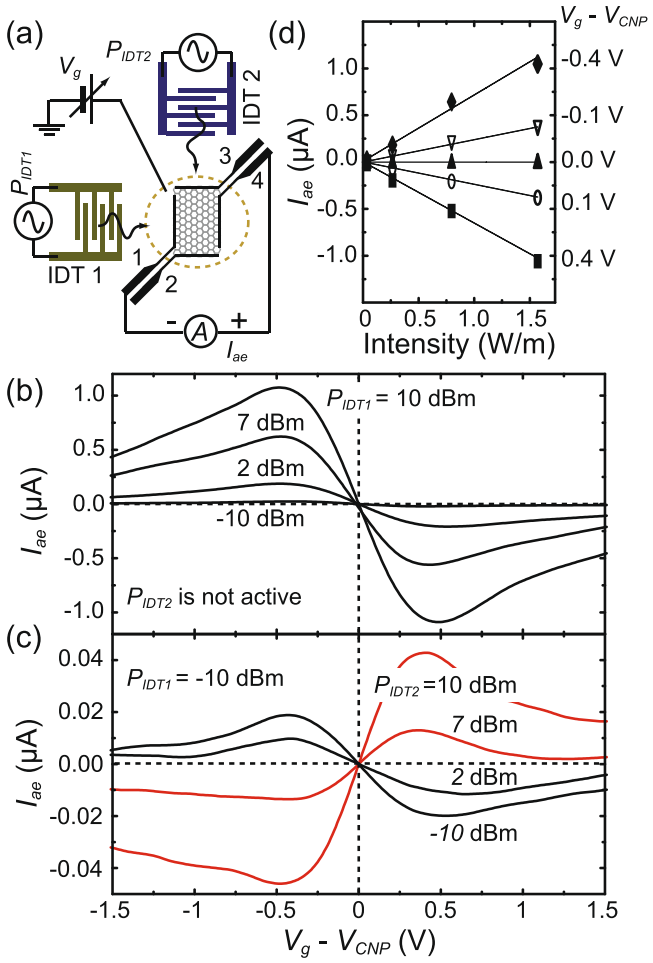

Figure 3. Acoustoelectric characteristics of the device. (**a**) The schematic plot of the I_{ae} measurement setup. (**b**) The quiescent performance of acoustoelectric current I_{ae} as a function of V_g at different RF-power P_{IDT1} applied on ITD1 at 191 MHz. Note that IDT2 remains unactivated. The majority carriers change from p- to n- type as the Fermi level is tuned across CNP, which causes a sign reversal of I_{ae}. (**c**) I_{ae} versus V_g traces with various P_{IDT2} applied on IDT2. Here P_{IDT1} is kept at −10 dBm and both IDTs are operated at 191 MHz. When P_{IDT2} increases larger than 2 dBm, the polarity of measured I_{ae} changes. (**d**) Acoustoelectric current as a function of P_{IDT1} at various V_g. Data are extracted from (**b**).

is directly recorded through a digital oscilloscope with a bandwidth of 100 MHz and a sampling rate up to 1 GHz. The output voltage V_{SAW} corresponding to $I_{ae} \sim 1\ \mu$A is approximately 1 μV. The RF-power P_{IDT2} is amplitude modulated by a square wave with a period $T_m(=1/f_m = 100\ \mu$s) and a duty cycle $D(=0.2)$. Oscilloscope traces of the applied RF-signal on IDT2 is shown in Fig. 4(b) for reference. Figure 4(c) shows the screen shot of the output waveforms of I_{ae} taken from the oscilloscope at various P_{IDT2}. As P_{IDT2} is within active time of the pulse, I_{ae} exhibits a dip feature due to the cancellation by negative I_{ae}. As P_{IDT2} increases up to 6 dBm, I_{ae} is nearly vanished. Here the GAET functions as an active-High logic switch that processes information as either a "1" or a "0", depending on whether the switch is off − getting finite acoustoelectric current I_{ae}− or on − I_{ae} measured zero. We estimate the on/off ratio of I_{ae} is approximately 10^4 based on the noise level of the on and off states.

To characterize the response time of switching I_{ae}, we note that the maximum switching rate - the key parameter to limit sampling rate in digital communications - is determined by the transition time of I_{ae} in response to the modulated RF pulse. We can switch I_{ae} simply by modulating RF signal applied on a single IDT. Unlike the dual-SAW scheme discussed above, one can view such operation as an active-Low logic switch. In terms of GFET, graphene provides a nature 2D conducting channel such that a digital on/off state can be simply achieved by modulating the source-drain bias without applying a gate voltage, if the signal gain is not a concern. On the other hand, a RF signal can be directly converted to an electric signal in GAET. In this regard, GAET has an advantage over GFET as a logic switch. Figure 5(a) shows the circuit diagram to switch I_{ae} by operating IDT1 alone. Figure 5(b) shows the detailed profile of the I_{ae} pulse waveform generated by a square wave-modulated $P_{IDT1}(=17$ dBm). The on-time t_{on} is set about 20 μs. Based on the 90% and 10% threshold levels of the pulse amplitude, we determine the Rise t_R and Fall t_F time to be about ~6 μs. Figure 5(c) shows the evolution of I_{ae} with different modulation frequencies. For comparison, we normalize I_{ae} to its quiescence value $I_0(=1.6\ \mu$A), and time to the modulated period T_m. As displayed in Fig. 5(c), the on-state remains stable with T_m up to 20 μs, corresponding to

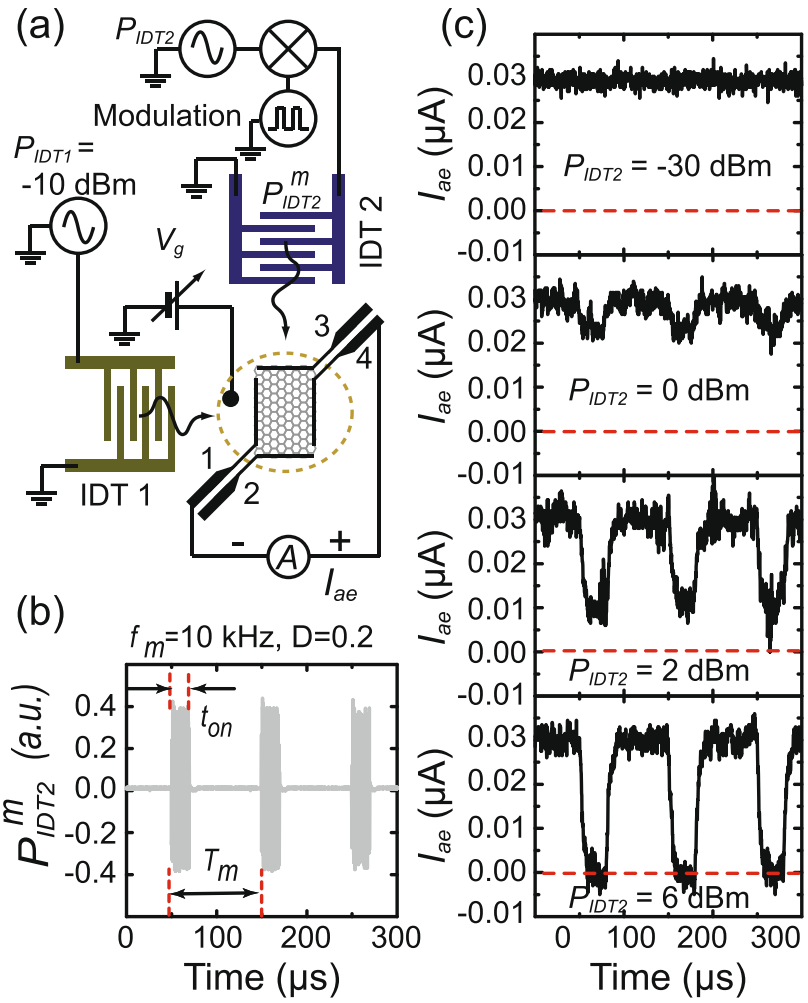

Figure 4. Time-resolved measurement of acoustoelectric current I_{ae}. (**a**) Schematic diagram of the measurement circuit. Graphene is biased in the hole-rich regime at $V_g - V_{CNP} = -0.5$ V. (**b**) The time dependence of the amplitude modulated P_{IDT2} with a duty ratio $D(\equiv t_{on}/T_m) = 0.2$, where $T_m(=1/f_m)$ is the modulation period. (**c**) The time dependence of I_{ae} with different modulated P_{IDT2} ranging from −30 dBm to 6 dBm. Here both IDTs is excited at 190 MHz. P_{IDT1} is fixed at ~−10 dBm, and P_{IDT2} is modulated with frequency $f_m = 10$ kHz.

dynamic switch rate of 50 kHz. That is to say, the peak value of the I_{ae} waveform with a pulse width ~4 μs is within 90% of the full amplitude. The propagation delay time t_p - a parameter to evaluate the jitter effects- is about 0.6 μs. We find $t_p \sim \ell/v_s$, where ℓ(~ 1.4 mm) is the separation between IDT1 and the center of graphene. We estimate the digital modulation rate of ~10 KB/s for the GAET switch.

Data shown in Figs 4(c) and 5(c) present a way to switch on/off channel current by the digitized RF power without resorting the gate voltage, as long as graphene is intentionally doped away from the CNP. The liquid gate is not necessary for the GAET switch. On the other hand, we have affirmed that the switch rate is not affected by the presence of the ionic liquid nor the instrument. We estimate the capacitance of a single IDT C_{IDT} ~ 6.25 pF and the circuit input impedance around 448 Ω, giving rise to the RC time constant around 2.8 ns, which is much shorter than the t_R and t_F measured. Therefore, we argue that the intrinsic RC delay is likely due to the impedance mismatch. We conceive the switching rate can be immediately raised up by shrinking the channel width of graphene. To optimize impedance-matching one may employ tapered IDTs, functioning as an impedance-transformer[38–40], which impedance match to 50 Ohm transmission line at one end and to the characteristic impedance of the tailored graphene and the leads at other end. To this end, one also needs to characterize the output impedance of GAET and match it with that of the transmission line extended to the measurement ports.

The dynamics of acoustoelectric effects of emerging post-graphene 2D materials – e.g. transition metal dichalcogenides (TMDs) and black phosphorus (BP) are much less explored[41] and would be interesting subjects for future studies.

Finally, we wish to make few comments on future development of GAET logic devices. The ultimate response time of the GAET switch is limited by the SAW velocity v_s and the channel width. There are several approaches to increasing the switching rate. One may try to fabricate the device on substrates with a relatively large electromechanical coupling coefficient, e.g. 42° Y-X $LiTaO_3$ or 64° Y-X $LiTaO_3$ substrate, which have been widely applied to

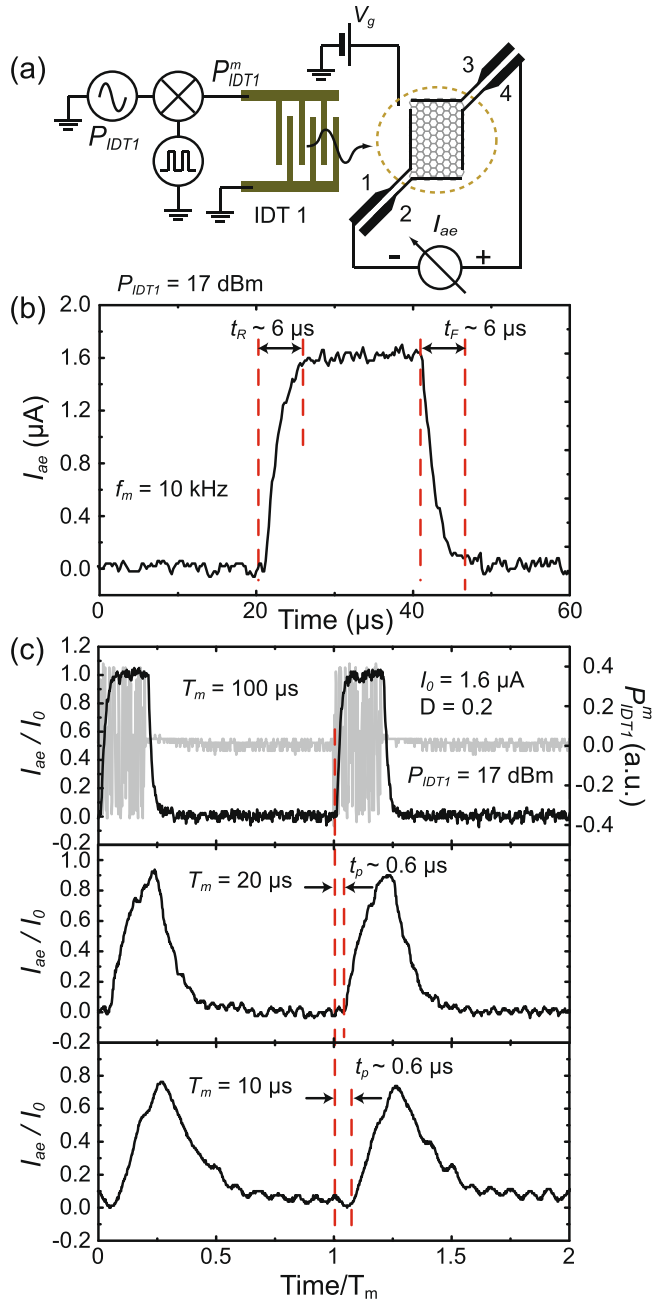

Figure 5. Characteristics of the transition rate of the graphene acoustoelectric switch. (**a**) Circuit diagram for the measurement. IDT1 is activated by a square wave-modulated RF-signal P^m_{IDT1}, where IDT2 is inactive. (**b**) A representative waveform of I_{ae} illustrates the step response of the device. Here t_{on} is set to be 20 μs and the Rise t_R and Fall t_F time is found to be about 6 μs. (**c**) The time dependence of I_{ae} with power modulation period of 100 μs, 20 μs, and 10 μs. Here P_{IDT1} is fixed at 6 dBm and the duty cycle $D = 0.2$. The gray trace shown in the upper panel is the time trace of the modulated RF-signal P^m_{IDT1} applied on IDT1. To compare how the transition response of I_{ae} digital pulse evolves with different T_m, I_{ae} is normalized to its peak value I_0(=1.6 μA), and the time scale is normalized to T_m.

the SAW devices for mobile communications. However, the tradeoff is that larger leaky wave may yield a lower I_{ae}. In principle, a high-slew rate of I_{ae} can be obtained from a wide-band SAW device, which can be implemented by an apodized IDT design or simply reducing the number of fingers in the IDT. A narrower channel width may give a shorter response time, but it in turn reduces I_{ae} or requires a larger P_{IDT}. This drawback makes GAET unsuitable for latch operation. Regarding the operation scheme, a single IDT is sufficient for the active-Low switch. Using collinear dual IDTs such as IDT1 and IDT3 (or IDT2 and IDT4), one can apply lower and balanced P_{IDT} for the active-High switch. Nevertheless, evident interference due to reflected waves should be taken into account. For the dual-SAW operation, two SAWs can be excited at different frequencies. However, it makes SAW attenuation become more pronounced at a higher frequency. In addition, by properly utilizing four leads and IDTs, we can

directly measure I_{ae} to make GAET act as an acoustoelectric branch switch[28]. We note that recent studies reveal several intriguing interface elastic properties of van der Waals materials[42–44] and may offer a mean to speed up the switch rate of GAET by engineering the interfacial acoustoelectric properties. Maybe the switch rate is slow (audio frequencies) and the design is a little complex, we think that the GAET opens a route for developing graphene-based logic switch. In this work, we only demonstrate the feasibility of GAET as a logic switch and leave aforementioned issues for future studies.

Conclusion

In conclusion, we present an accessible operation scheme of GAET for a logic switch with a moderate on/off rate of ~10^4 at room temperature. By manipulating the propagation direction of I_{ae}, the measured values of I_{ae} can be fine tuned to zero - an ideal off state for a logic switch. We demonstrate the dynamic switch rate of I_{ae} can be up to 50 kHz by modulating the amplitude of the input RF-signal applied on IDTs. By deliberately controlling the digitized RF-power applied on a pair of crossed-IDT or a single IDT, the output I_{ae} can be either active-High or active-Low, respectively. The digital modulation rate can achieve ~10 KB/s. The performance of the GAET is suitable for processing digital audio signals. Even the switch rate is slow, our work provides a means to integrate the SAW device and the acoustoelectric effects for future development of graphene-based logic devices.

References

1. Castro Neto, A. H., Guinea, F., Peres, N. M., Novoselov, K. S. & Geim, A. K. The electronic properties of graphene. *Rev. Mod. Phys.* **81**, 109 (2009).
2. Schwierz, F. Graphene transistors. *Nat Nano* **5**, 487 (2010).
3. Lin, Y.-M. *et al*. Wafer-scale graphene integrated circuit. *Sci.* **332**, 1294 (2011).
4. Han, S.-J., Valdes G., A., Oida, S., Jenkins, K. A. & Haensch, W. Graphene radio frequency receiver integrated circuit. *Nat. Commun.* **5**, 3086 (2014).
5. Petrone, N., Meric, I., Chari, T., Shepard, K. L. & Hone, J. Graphene field-effect transistors for radio-frequency flexible electronics. *IEEE J. Electron Devices Soc.* **3**, 44 (2015).
6. Cartwright, J. Intel enters the third dimension. *Nat. News*, https://doi.org/10.1038/news.2011.274 (6 May 2011).
7. Fiori, G. *et al*. *Nat Nano* **9**, 768 (2014).
8. Han, M. Y., Özyilmaz, B., Zhang, Y. & Kim, P. Energy band-gap engineering of graphene nanoribbons. *Phys. Rev. Lett.* **98**, 206805 (2007).
9. Li, X., Wang, X., Zhang, L., Lee, S. & Dai, H. Chemically derived, ultrasmooth graphene nanoribbon semiconductors. *Sci.* **319**, 1229–1232, https://doi.org/10.1126/science.1150878 (2008).
10. Campbell, C. *Surface acoustic wave devices and their signal processing applications*. (Academic press, London, 1989).
11. Campbell, C. K. *Surface Acoustic Wave Devices for Mobile and Wireless Communications*. (Academic Press, Inc., 1998).
12. Harris, C. M. Seeing saw potential. *Anal. Chem.* **1**, 355 A (2003).
13. Wixforth, A. *et al*. Surface acoustic waves on gaas/al$_x$ga$_{1-x}$ as heterostructures. *Phys. Rev. B* **40**, 7874–7887 (1989).
14. Willett, R. L. *et al*. Anomalous sound propagation at $\nu = 1/2$ in a 2d electron gas: Observation of a spontaneously broken translational symmetry? *Phys. Rev. Lett.* **65**, 112–115 (1990).
15. Esslinger, A. *et al*. Ultrasonic approach to the integer and fractional quantum hall effect. *Surf. Sci.* **305**, 83–86 (1994).
16. Shilton, J. M. *et al*. Effect of spatial dispersion on acoustoelectric current in a high-mobility two-dimensional electron gas. *Phys. Rev. B* **51**, 14770–14773 (1995).
17. Thalmeier, P., Dóra, B. & Ziegler, K. Surface acoustic wave propagation in graphene. *Phys. Rev. B* **81**, 041409 (2010).
18. Miseikis, V., Cunningham, J. E., Saeed, K., O'Rorke, R. & Davies, A. G. Acoustically induced current flow in graphene. *Appl. Phys. Lett*. **100** (2012).
19. Santos, P. V., Schumann, T., Oliveira, M. H., Lopes, J. M. J. & Riechert, H. Acousto-electric transport in epitaxial monolayer graphene on sic. *Appl. Phys. Lett*. **102** (2013).
20. Zhang, S. H., Xu, W., Badalyan, S. M. & Peeters, F. M. Piezoelectric surface acoustical phonon limited mobility of electrons in graphene on a gaas substrate. *Phys. Rev. B* **87**, 075443 (2013).
21. Bandhu, L., Lawton, L. M. & Nash, G. R. Macroscopic acoustoelectric charge transport in graphene. *Appl. Phys. Lett*. **103** (2013).
22. Bandhu, L. & Nash, G. R. Controlling the properties of surface acoustic waves using graphene. *Nano Res.* **9**, 685–691 (2015).
23. Tang, C.-C., Chen, Y.-F., Ling, D. C., Chi, C. C. & Chen, J.-C. Ultra-low acoustoelectric attenuation in graphene. *J. Appl. Phys.* **121**, 124505 (2017).
24. Chen, Y. *et al*. Acoustically induced current in graphene by aluminum nitride transducers. *Appl. Phys. Lett.* **108**, 033107, https://doi.org/10.1063/1.4940400 (2016).
25. Okuda, S. *et al*. Graphene surface acoustic wave sensor for simultaneous detection of charge and mass. *ACS Sensors* **3**, 200 (2018).
26. Zhang, S. H. & Xu, W. Absorption of surface acoustic waves by graphene. *AIP Adv.* **1**, 022146 (2011).
27. Ozcelik, A. *et al*. Acoustic tweezers for the life sciences. *Nat. Methods* **15**, 1021 (2018).
28. Talyanskii, V. I., Graham, M. R. & Beere, H. E. Acoustoelectric y-branch switch. *Appl. Phys. Lett.* **88**, 083501 (2006).
29. Lane, J. R. *et al*. Flip-chip gate-tunable acoustoelectric effect in graphene. *J. Appl. Phys*. **124**, 194302, https://doi.org/10.1063/1.5047211 (2018).
30. Weinreich, G. Acoustodynamic effects in semiconductors. *Phys. Rev.* **104**, 321–324 (1956).
31. Efros, A. L. & Galperin, Y. M. Quantization of the acoustoelectric current in a two-dimensional electron system in a strong magnetic field. *Phys. Rev. Lett.* **64**, 1959–1962 (1990).
32. Friend, J. & Yeo, L. Y. Microscale acoustofluidics: Microfluidics driven via acoustics and ultrasonics. *Rev. Mod. Phys.* **83**, 647–704 (2011).
33. Das, A. *et al*. Monitoring dopants by Raman scattering in an electrochemically top-gated graphene transistor. *Nat. Nanotechnol*. **3**, 210 (2008).
34. Wong, K. K. *Properties of Lithium Niobate*. (INSPEC, 1989).
35. Tang, C.-C., Li, M.-Y., Li, L. J., Chi, C. C. & Chen, J. C. Characteristics of a sensitive micro-hall probe fabricated on chemical vapor deposited graphene over the temperature range from liquid-helium to room temperature. *Appl. Phys. Lett*. **99** (2011).
36. Tang, C.-C., Li, M.-Y., Li, L. J., Chi, C. C. & Chen, J.-C. Graphene-gaas/alxga1-xas heterostructure dual-function field-effect transistor. *Appl. Phys. Lett*. **101** (2012).
37. Li, M.-Y. *et al*. Charged impurity-induced scatterings in chemical vapor deposited graphene. *J. Appl. Phys.* **114**, 233703 (2013).
38. White, T. C. *et al*. Traveling wave parametric amplifier with josephson junctions using minimal resonator phase matching. *Appl. Phys. Lett.* **106**, 242601, https://doi.org/10.1063/1.4922348 (2015).
39. Roy, T. *et al*. Broadband parametric amplification with impedance engineering: Beyond the gain-bandwidth product. *Appl. Phys. Lett.* **107**, 262601, https://doi.org/10.1063/1.4939148 (2015).

40. Mosallaei, H. & Sarabandi, K. Antenna miniaturization and bandwidth enhancement using a reactive impedance substrate. *IEEE Transactions on Antennas Propag.* **52**, 2403–2414, https://doi.org/10.1109/TAP.2004.834135 (2004).
41. Zheng, S., Wu, E. & Zhang, H. Anomalous acoustoelectric currents in few-layer black phosphorus nanocrystals. *IEEE Transactions on Nanotechnol.* **17**, 590–595, https://doi.org/10.1109/TNANO.2018.2827666 (2018).
42. Ge, S. *et al*. Coherent longitudinal acoustic phonon approaching thz frequency in multilayer molybdenum disulphide. *Sci. Reports* **4**, 5722 (2014).
43. Beardsley, R. *et al*. Nanomechanical probing of the layer/substrate interface of an exfoliated inse sheet on sapphire. *Sci. Reports* **6**, 26970 (2016).
44. Greener, J. D. G. *et al*. Coherent acoustic phonons in van der waals nanolayers and heterostructures. *Phys. Rev. B* **98**, 075408, https://doi.org/10.1103/PhysRevB.98.075408 (2018).

Acknowledgements

This work was supported by Ministry of Science and Technology, Taiwan under Grant No. MOST 107-2112-M-007-003-MY3, MOST 107-2811-M-007-1052- and MOST 107-2627-E-002-002-, and also supported by the Center for Quantum Technology from the Featured Areas Research Center Program within the framework of the Higher Education Sprout Project by the Ministry of Education (MOE) in Taiwan under Grant No. 107-3017-F-007-001.

Author Contributions

Ching-Ping Lee measured the experimental data, analyzed the data, and drew all figures. Yu-Peng Hong fabricated the devices, measured the experimental data. Man-Ting Shen manufactured the measurement probe. Chiu-Chun Tang designed the study and set up the measurement system. Cen-Shawn Wu gave the idea about designing and fabricating devices. D.C. Ling, Yung-Fu Chen, Cen-Shawn Wu, Jeng-Chung Chen wrote the manuscript. Jeng-Chung Chen also supervised all portions. All authors reviewed the manuscript.

Additional Information

Competing Interests: The authors declare no competing interests.

Publisher's note: Springer Nature remains neutral with regard to jurisdictional claims in published maps and institutional affiliations.